

**AJP**

ISSN : 0971 - 3093

Vol 27, Nos 9 -12, September-December 2018

# ASIAN JOURNAL OF PHYSICS

**An International Research Journal**

Advisory Editors : W. Kiefer & FTS Yu



Toshimitsu Asakura

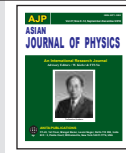


ap

**ANITAPUBLICATIONS**

FF-43, 1st Floor, Mangal Bazar, Laxmi Nagar, Delhi-110 092, India

B O : 2, Pasha Court, Williamsville, New York-14221-1776, USA



## Effects of detection area on measurements of spectral reflectance in human skin tissue

Tomonori Yuasa<sup>1</sup>, Yuta Kobori<sup>1</sup>, Kaustav Das<sup>1</sup>, Takaaki Maeda<sup>2</sup>,  
Hideki Funamizu<sup>1</sup>, and Yoshihisa Aizu<sup>1</sup>

<sup>1</sup>Muroran Institute of Technology, Muroran, Hokkaido 050-8585, Japan

<sup>2</sup>Kushiro National College of Technology, Kushiro, Hokkaido 084-0916, Japan

This article is dedicated to Prof T Asakura

Measurement of spectral reflectance of skin is influenced by the size of the detection area in a spectrophotometer. We investigate changes in the spectral reflectance curve and photon fluence in a visible wavelength range by using Monte Carlo simulation of light propagation in a nine-layered skin tissue model. Reflected light component in the longer wavelength range broadens on the skin surface, and is subject to be missed if the detecting aperture is small. This component should be detected properly enough to measure accurate spectral reflectance. An experiment was conducted to discuss spectral characteristics with respect to size of the detection area. © Anita Publications. All rights reserved..

**Keywords:** spectral reflectance, human skin, Monte Carlo simulation

### 1 Introduction

Light propagation in biological media is interesting physical phenomenon. Human body is especially an important medium in which light is absorbed and scattered in the wavelength-dependent manner. In a visible (VIS) to near-infrared (NIR) range of wavelength, light is known to penetrate in the human tissue in depth of 1~3 mm [1]. This region corresponds successfully to human skin tissue. From this nature, light propagation in human skin tissue have received much attention from researchers who study and develop techniques for measuring concentrations of chromophores such as melanin and hemoglobin [2, 3], tissue structural abnormality [4-6], and skin color [7]. These give useful information for dermatology and cosmetic industry.

In general, propagation of light in VIS-NIR wavelength is investigated by spectrophotometry which gives spectral reflectance. By this typical instrumental approach, many researchers studied method for estimating melanin and hemoglobin concentration and blood oxygenation dynamics [2, 3, 7] on the basis of the multi-variate analysis of spectral reflectance. Various types of spectrophotometric systems are commercially available and can easily be used for spectral reflectance measurements.

It should be noticed, however, that measured spectral reflectance contains contribution of light component coming back from an object and condition of measurements depends on property of light diffusion inside the object. Most direct measuring condition relating to the light diffusion is a size of a detecting aperture and secondary an area of illumination. When the skin spectral reflectance is measured, the size of a detecting aperture should appropriately be set by considering diffusion properties of light in skin tissue. However, general-purpose spectrophotometer contains only two or three preset sizes of the detecting aperture. Therefore, the necessary size should be investigated for appropriate use of the spectrophotometer which is specific to human skin tissue.

Corresponding author :

e-mail: [yuasa@mmm.muroran-it.ac.jp](mailto:yuasa@mmm.muroran-it.ac.jp) (Tomonori Yuasa) and [aizu@mmm.muroran-it.ac.jp](mailto:aizu@mmm.muroran-it.ac.jp) (Yoshihisa Aizu)

In this paper, we investigate the effect of a detecting aperture size on measurements of spectral reflectance in human skin tissue both by numerical simulation and by experiment. For this, we employed Monte Carlo simulation of light propagation in a layered skin tissue model [8], and discussed results of simulated spectral reflectance and photon fluence map. A result of experiment with an integrating sphere demonstrates the same tendency with that of the simulation, though values of reflectance changes are different between simulation and experiment.

## 2 Model of light propagation in skin tissue

### 2.1 Skin tissue model

Skin tissue has complex structure which is inhomogeneous and shaped irregularly, and has anisotropic physical properties. From a histological point of view, skin tissue is often considered by multi-layered structure which is useful for numerical modelling. Though the conventional studies generally employ a three-layered model consisting of epidermis, dermis, and subcutaneous fat tissue, we developed a nine-layered skin tissue model [9] on the basis of detailed histological knowledge. Figure 1 shows (a) schematic cross section of skin tissue structure, (b) its nine-layered model, and (c) the conventional three-layered model. In Fig. 1(b), the skin tissue is classified into nine parallel layers. From top to bottom, there are stratum corneum ( $L_1$ ), stratum granulosum/ stratum spinosum ( $L_2$ ), stratum basale ( $L_3$ ), papillary dermis ( $L_4$ ), subpapillary dermis ( $L_5$ ), upper blood net dermis ( $L_6$ ), reticular dermis ( $L_7$ ), deep blood net dermis ( $L_8$ ), and subcutaneous tissue ( $L_9$ ). Typical thickness of each layer is given by literatures [6, 9-12]. Concentrations of chromophores such as melanin in epidermis and oxygenated or deoxygenated hemoglobin in dermis and subcutaneous tissue are the main factors which influence the properties of light absorption in skin tissue. Cells and fiber components such as blood cells, collagen, and elastin are closely related to light scattering properties due to difference in refractive index. In our model, we assume that absorption and scattering properties are uniform in each of the nine layers. The nine-layered skin tissue model is successfully used for Monte Carlo simulation of light propagation. By setting of values for necessary optical and geometrical parameters in each layer, realistic spectral reflectance curves and visual photon fluence distributions are obtained.

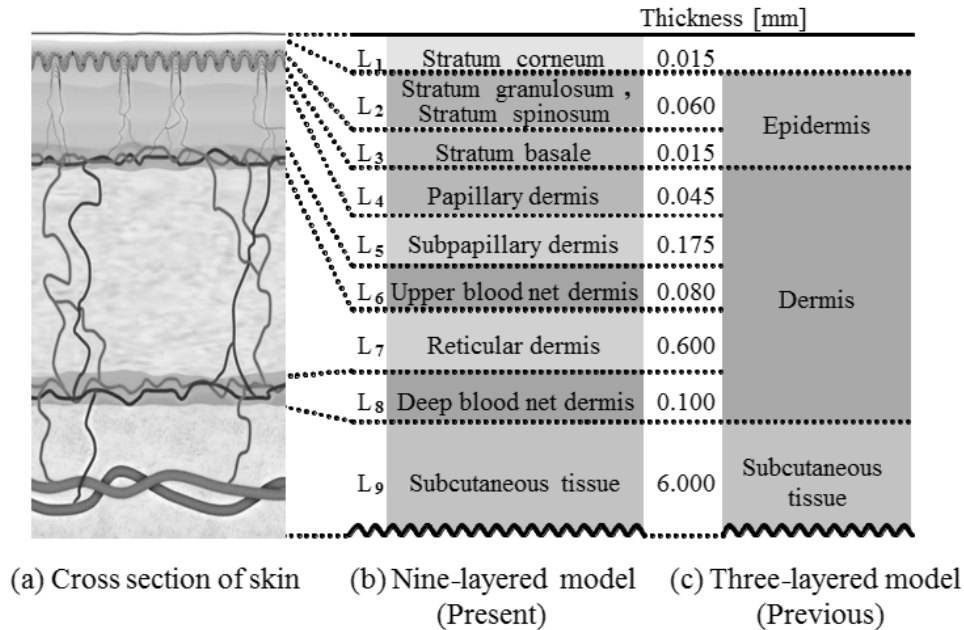


Fig 1. Schematic structure of skin tissue, nine-layered model, and three layered model.

## 2.2 Monte Carlo simulation

Figure 2 shows a concept of Monte Carlo simulation (MCS) for light propagation in multi-layered tissue [8]. The MCS treats light as a bundle of photons. A photon with weight of 1 is launched into the skin tissue at the origin of  $x$ ,  $y$ , and  $z$  axes, and traveling of photon inside the skin is calculated. The photon traveling is calculated step by step in the computer. Each step is specified by its length  $L$ , deflection angle  $\theta$ , and azimuthal angle  $\psi$ . To determine these values, we used the algorithm of Wang *et al* [8], in which five input parameters must be specified at a given wavelength  $\lambda$  for each layer: scattering coefficient  $\mu_s(\lambda)$ , absorption coefficient  $\mu_a(\lambda)$ , anisotropy scattering parameter  $g(\lambda)$ , refractive index  $n(\lambda)$ , and thickness  $t$ . We employed typical values for these five parameters that are published in literature [6, 9-12].

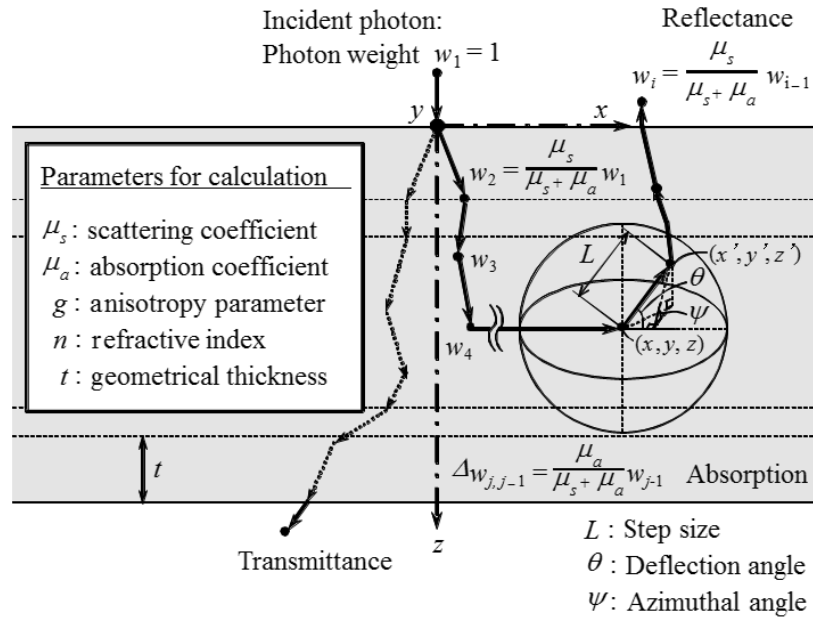


Fig 2. Concept of Monte Carlo simulation of light propagation in multi-layered tissue.

A traveling length in which the photon undergoes neither an absorbing event nor a scattering event is considered as a free path length. After traveling the path length of one step, the photon weight is attenuated at a rate determined by absorption and scattering coefficients. This step-like propagation is repeated by continuous generation of random numbers. When traveling on many steps and the resultant weight is smaller than a preset threshold ( $10^{-6}$  in this paper), then this photon is regarded as negligibly attenuated, and the second photon enters the tissue. By accumulating values of the weight that are re-emitted from the top surface, reflectance is calculated with reference to the total values of incident photon weight. We used  $10^6$  photons to obtain a stable reflectance result at each wavelength. This process is carried out at each of the necessary wavelength points, and finally spectral reflectance is obtained. We took the process in the wavelength range 380-780 nm at an interval of 10 nm.

During the MCS process mentioned above, the computer records and stores all the values of the photon weight with its position in the three-dimensional manner. Thus, the MCS algorithm [8] used in this paper provides the amount of light absorption in each volume element of the skin tissue model. This amount is referred to as photon fluence  $\phi$  [8] given by

$$\phi [i_x, i_y, i_z] = \frac{A[i_x, i_y, i_z]}{\mu_a} [\text{cm}^{-2}] \quad (1)$$

where  $A$  denotes the amount of light absorption per unit volume, and  $i_x$ ,  $i_y$ , and  $i_z$  indicate the element number of each grid in the horizontal ( $i_x$ ,  $i_y$ ) and vertical ( $i_z$ ) directions in the numerical skin tissue model. Here, we investigate the fluence in  $x$ - $z$  plane with  $y = 0$ , in this paper.

We have two different modes in the calculation of photon fluence. One is the total fluence which include all the reflected, absorbed, and transmitted components of light, and another is the detected fluence which contains only reflected component returning to the skin surface. The latter fluence presents light component which is measurable instrumentally on the skin surface. Both these two can visually be expressed by illustration as energy distribution pattern of light propagation.

### 3 Numerical Investigation

#### 3.1 Method and condition

A surface of a skin tissue model is designated by  $x$  and  $y$  axes, and a direction of penetration into the deep layers is given by  $z$  axis. As shown in Fig 3, photons of incident light are launched one by one into the tissue perpendicularly. We assumed three different types of an illuminating spot; a point-like illumination, a circular-spot illumination of diameter  $d_i = 2$  mm, and a circular spot of  $d_i = 4$  mm. As for the detection, we assumed circular areas of ten different diameters  $d = 0.2$ -40 mm. We also assumed that the photons re-emitted from the surface in all the directions in space are accounted for detection, which is the same condition as that used in experiments described later in this paper. No polarization is considered, but Fresnel reflection law is included in the algorithm.

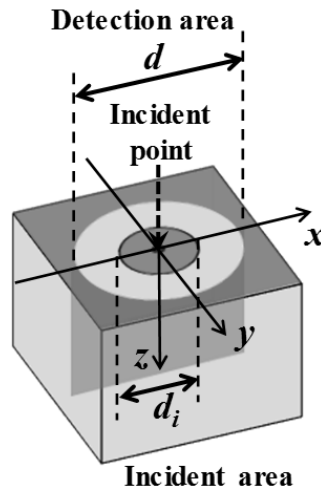


Fig 3. Definition of a point and area for illumination and detection on the skin surface.

#### 3.2 Point-like illumination

Figure 4 shows simulated spectral reflectance curves with various diameters of the detection area in the case of point illumination. Results with the large detection area having  $d = 6 - 40$  mm in diameter demonstrate no significant difference in the curves which are overlapped. With reducing the diameter  $d$ , reflectance is decreased especially in the longer wavelength range. Figure 5 demonstrates the photon fluence maps in  $x$ - $z$  plane for the case of 550nm wavelength. The map in (a) of Fig 5 gives the total fluence distribution, while that in (b), (c), and (d) give the detected fluence distributions. The latter maps are found to depend on diameter  $d$  of the detection area. Figure 6 demonstrates the photon fluence maps for a case of 700 nm wavelength in the same way as Fig 5. Comparison of the maps in Figs 5 and 6 demonstrates that light propagation broadens more widely and deeply inside the skin in 700 nm than in 550 nm. This property

indicates that light component penetrated into the deeper layers and diffused and coming back to the surface is not sufficiently detected in cases of using small diameters of the detecting aperture. This tendency is significant in the longer wavelength range in which light penetrates into the deeper and broadens widely in the skin tissue. It is found that the smaller area of detection is unacceptable for appropriate spectral reflectance measurements. The results of Figs 4 to 6 are specific to an ideal situation of the point-like illumination. More realistic situation is to use a circular-spot illumination.

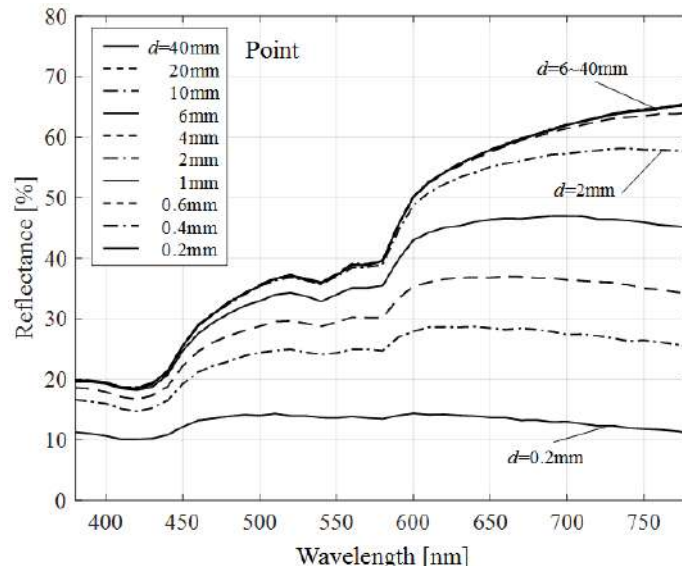


Fig 4. Simulated spectral reflectance curves with different diameters  $d$  of a detecting aperture for a point-like illumination.

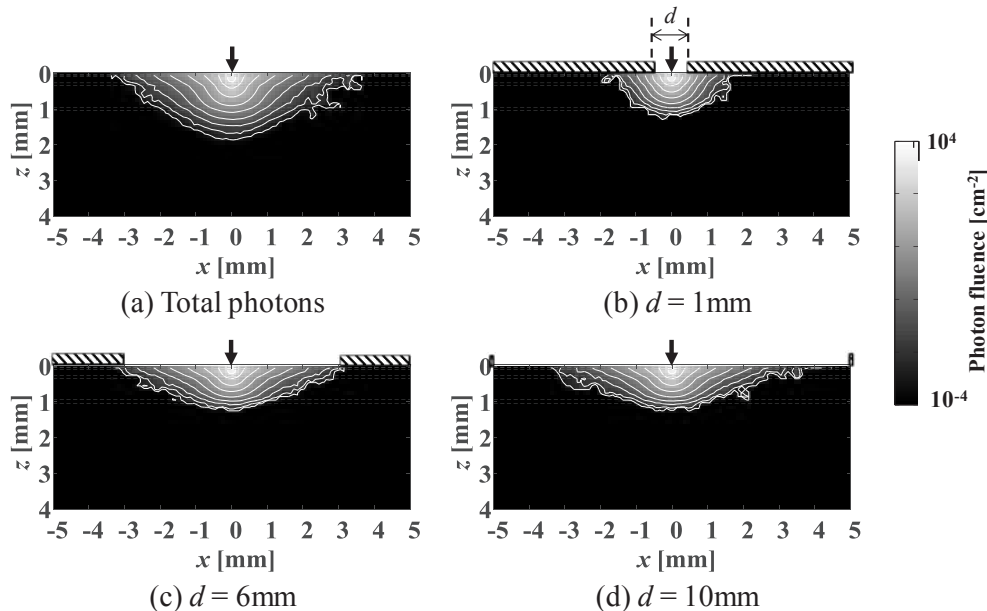
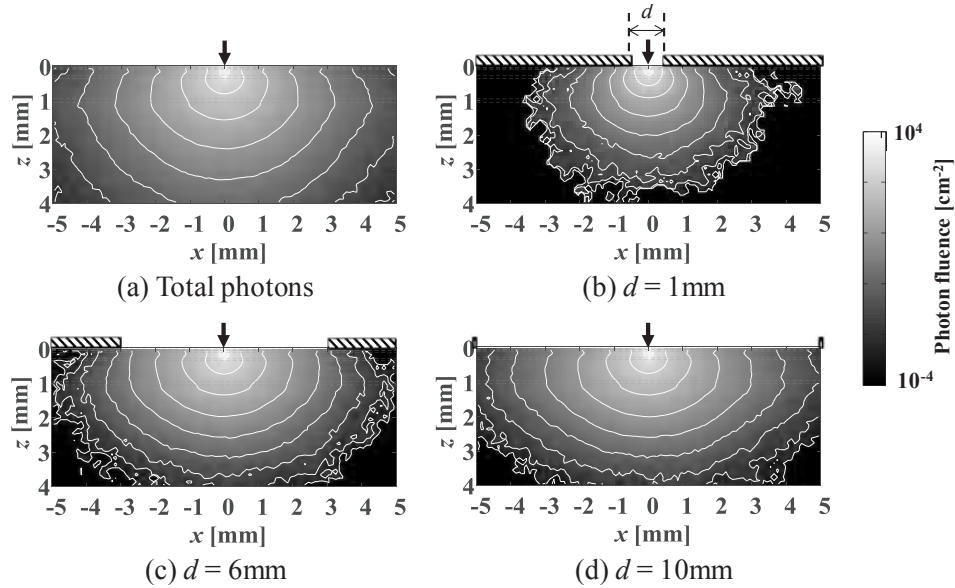


Fig 5. Two-dimensional distribution maps of (a) the total photon fluence and (b) – (d) the detected photon fluence with  $d = 1, 6,$  and  $10\text{mm}$  in diameter of the aperture, respectively, in  $550\text{ nm}$  wavelength of a point-like illumination.



**Fig 6.** Two-dimensional distribution maps of (a) the total photon fluence and (b) – (d) the detected photon fluence with  $d=1$ , 6, and 10 mm in diameter of the aperture, respectively, in 700 nm wavelength of a point-like illumination.

### 3.3 Circular-spot illumination

Figures 7 and 8 show simulated spectral reflectance curves with various diameters  $d$  of the detection area in cases of circular-spot illumination having  $d_i=2$  and 4 mm in diameter, respectively. In Fig 7, reflectance curves for  $d \leq 2$  mm are decreased more than those in Fig 4. This is probably due to insufficient detection area with respect to the diffused light component which is produced by  $d_i=2$  mm diameter illumination. In Fig 8, reflectance curves for  $d \leq 4$  mm are clearly reduced in the same way as those for  $d \leq 2$  mm in Fig 7. This is also because of insufficient diameter for the detection with respect to  $d_i=4$  mm diameter illumination.

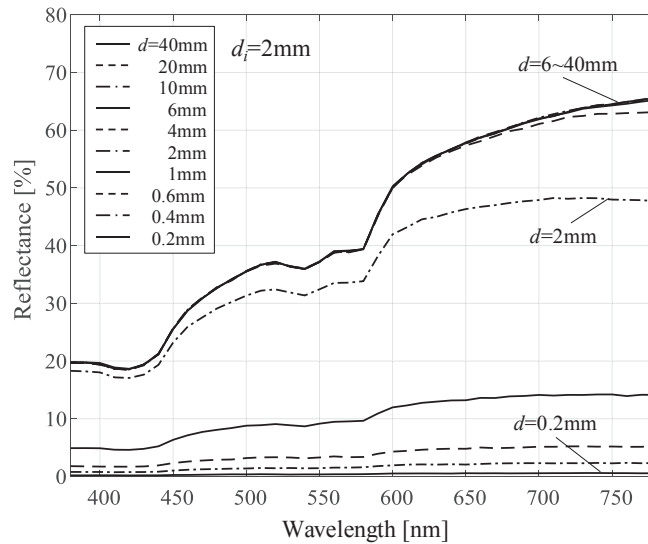


**Fig 7.** Simulated spectral reflectance curves with different diameters  $d$  of a detecting aperture for a circular spot illumination of  $d_i=2$  mm in diameter.

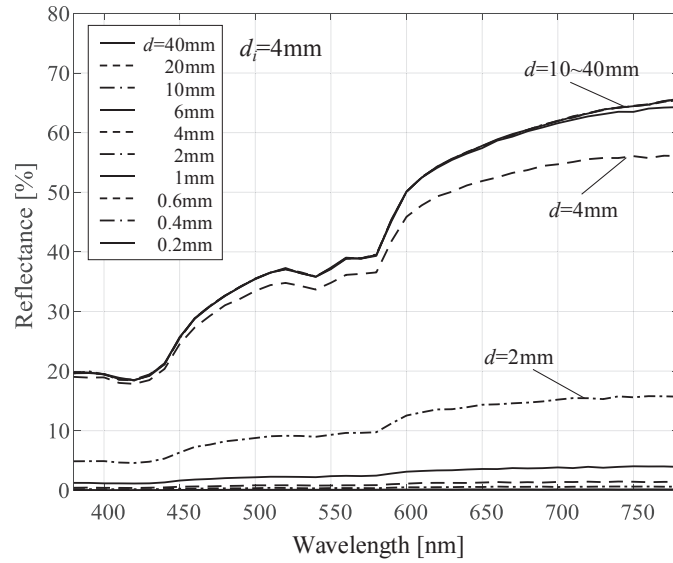


Fig 8. Simulated spectral reflectance curves with different diameters  $d$  of a detecting aperture for a circular spot illumination of  $d_i = 4$  mm in diameter.

Figures 9 and 10 give the photon fluence maps in 550 nm and 700 nm wavelength cases for  $d_i = 2$  mm circular spot illumination. The maps in (a) of Figs 9 and 10 show the total fluence while those in (b) to (d) show the detected fluence. By an areal illumination with  $d_i = 2$  mm in diameter, the photon fluence demonstrates horizontally broadened distribution in comparison with those of Figs. 5 and 6. The fluence maps in 700 nm are again found to be more widely diffused than those in 550 nm.

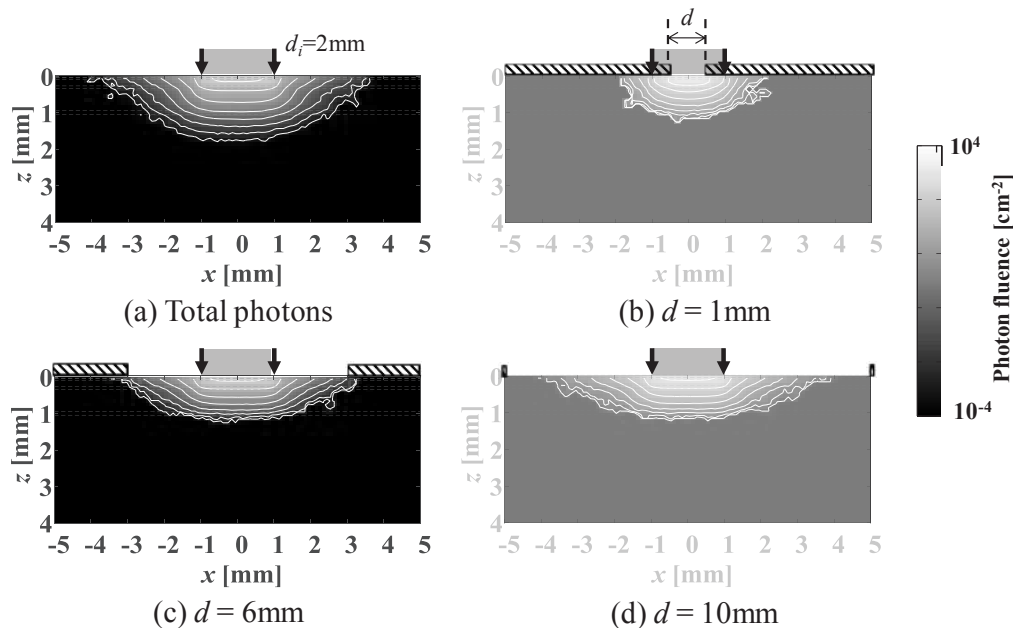
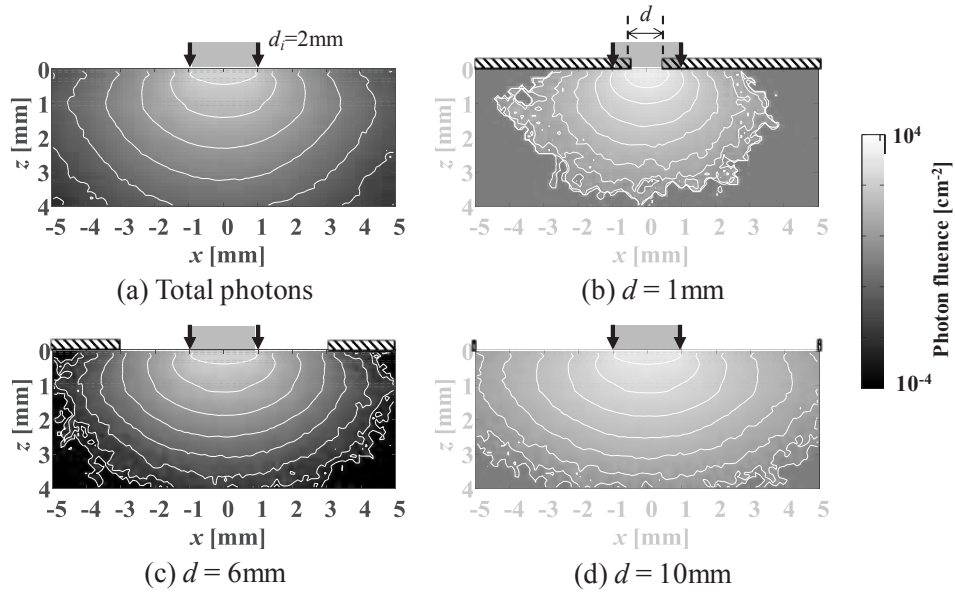
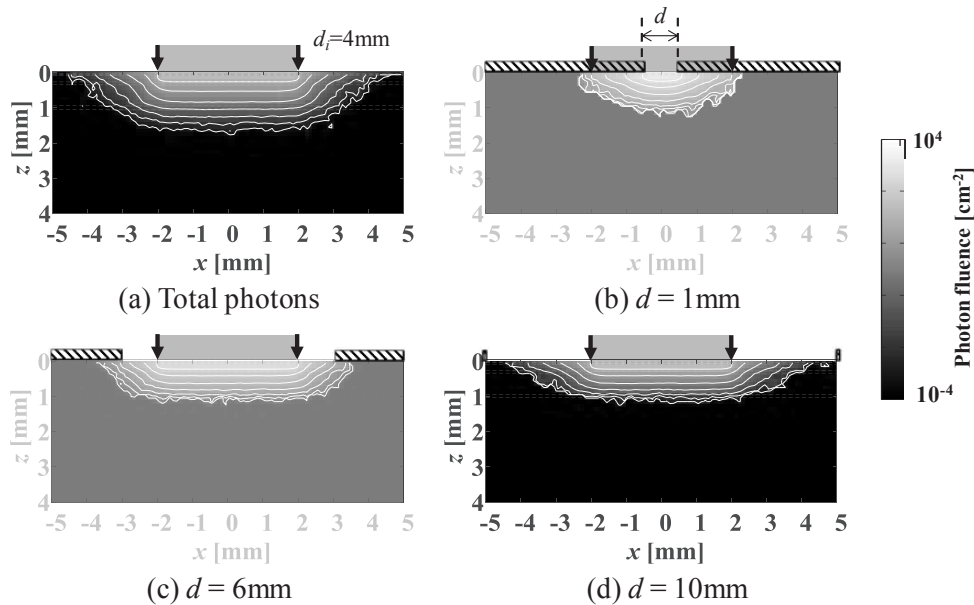


Fig 9. Two-dimensional distribution maps of (a) the total photon fluence and (b) – (d) the detected photon fluence with  $d = 1, 6,$  and  $10$  mm in diameter of the aperture, respectively, in 550 nm wavelength of a circular spot illumination of  $d_i = 2$  mm in diameter.



**Fig 10.** Two-dimensional distribution maps of (a) the total photon fluence and (b) – (d) the detected photon fluence with  $d = 1, 6,$  and  $10\text{mm}$  in diameter of the aperture, respectively, in  $700\text{ nm}$  wavelength of a circular spot illumination of  $d_i = 2\text{ mm}$  in diameter.

**Figures 11 and 12** show the maps in  $550$  and  $700\text{ nm}$  wavelength cases for  $d_i = 4\text{ mm}$  circular spot illumination. An increase of diameter from  $2$  to  $4\text{ mm}$  results in further broadening of the photon fluence distribution in a horizontal direction. The diameter  $d$  of  $6\text{ mm}$  or more in the detection area is probably necessary for receiving substantial amount of the diffused light component coming back to the surface.



**Fig 11.** Two-dimensional distribution maps of (a) the total photon fluence and (b) – (d) the detected photon fluence with  $d = 1, 6,$  and  $10\text{mm}$  in diameter of the aperture, respectively, in  $550\text{ nm}$  wavelength of a circular spot illumination of  $d_i = 4\text{ mm}$  in diameter.

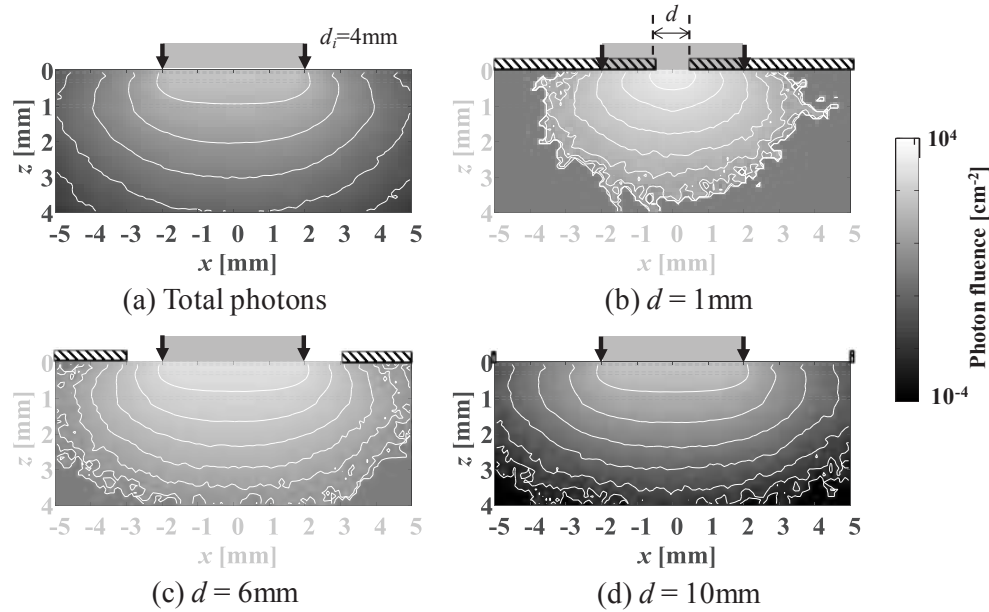


**Fig 12.** Two-dimensional distribution maps of (a) the total photon fluence and (b) – (d) the detected photon fluence with  $d=1, 6,$  and  $10\text{mm}$  in diameter of the aperture, respectively, in  $700\text{ nm}$  wavelength of a circular spot illumination of  $d_i=4\text{ mm}$  in diameter.

## 4 Experimental investigation

### 4.1 Method and apparatus

**Figure 13** shows a measuring apparatus for the spectral reflectance using an integrating sphere and spectrophotometer. Light from a halogen lamp source (Hayashi LA-150UX) was focused by lens to skin surface with a circular spot of  $d_i = 4\text{ mm}$  in diameter via a sample window of a 6-inch integrating sphere (Labsphere RT-060-SF). Diffusely reflected light from the skin was received at the detection port by a fiber probe having  $400\text{ }\mu\text{m}$  diameter. The detected area was changed by setting detecting aperture having diameters  $d = 4, 5, 6, 8, 10, 15,$  and  $22\text{ mm}$  on the sample window. The received light was transmitted into a multichannel spectrophotometer (Ocean optics USB-4000), which measures spectral reflectance in a visible wavelength range of  $380\text{-}780\text{ nm}$ .

### 4.2 Results

**Figure 14** shows spectral reflectance curves measured by different diameters  $d$  of the detecting aperture on the human forearm skin. Measured reflectance decreases as the detecting aperture becomes small. This decrease is significant in the wavelength range longer than  $600\text{ nm}$ . The curves with  $d = 10, 15,$  and  $22\text{ mm}$  seem to have almost the same behavior. The absolute values in reflectance are different between simulated curves in **Fig.8** and measured ones in **Fig 14** for the same detecting aperture diameter. However, the simulation and measurement demonstrate the same reduction behavior in reflectance especially in the longer wavelength range with insufficient size of the detection area. It can be seen that the appropriate diameter of a detecting aperture is estimated to be  $10\text{ mm}$  or more from both the simulated and measured results in case of  $d_i = 4\text{ mm}$  spot illumination. This estimation is of course dependent on the size of illuminating spot. However, a necessary margin of the detection area is supposed to be about  $4\text{ to }6\text{ mm}$  by considering the broadening in the diffused light in skin tissue. Therefore, the appropriate diameter for detection area is estimated to be the sum of illuminating spot diameter and this margin of  $4\text{ to }6\text{ mm}$  for human skin.

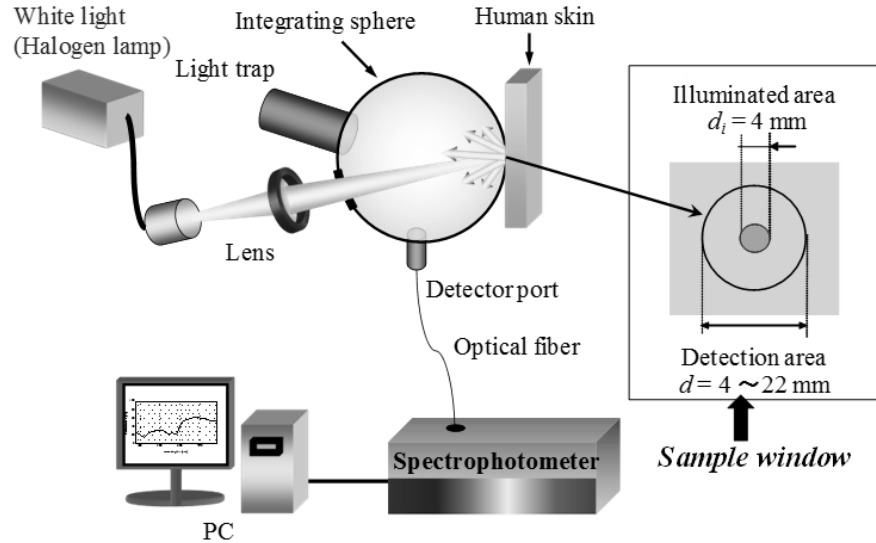


Fig 13. Measuring apparatus for spectral reflectance using a 6-inch integrating sphere.

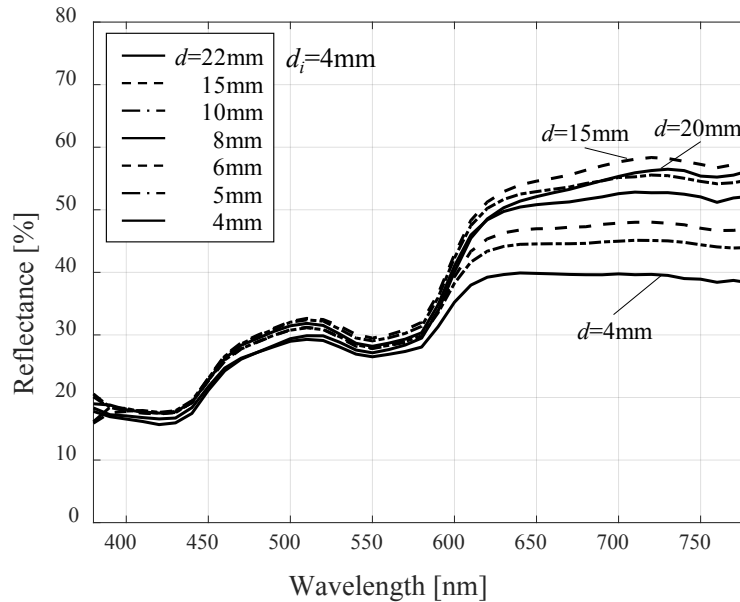


Fig 14. Measured spectral reflectance curves with different diameter  $d$  of a detecting aperture for a circular spot illumination of  $d_i = 4$  mm in diameter on a human forearm skin.

## 5 Conclusion

We investigated the effect of the detecting aperture size on measurements of spectral reflectance in human skin tissue both by Monte Carlo simulations and by spectrophotometric experiments. Undesirably small size of detecting aperture causes reduction of measured reflectance especially in the longer wavelength range. The necessary size is probably given by the sum of an illuminating spot size and a detection margin of 4 to 6 mm which results from the broadening of diffused light in the skin tissue. This estimation is useful for

reliable measurement of spectral reflectance in skin tissue in the fields of dermatology and cosmetic product development. The study presented in this paper is specific to human skin and may have some different properties for different objects to be measured. However, the same kind of investigation and discussion may be effective for the other objects.

## References

1. Tuchin V, *Tissue Optics: Light Scattering Methods and Instruments for Medical Diagnosis*. (SPIE-The International Society for Optical Engineering, Washington DC), 2000, Chap 1, p3.
2. Stratonnikov A A, Loschenov V B, *J Biomed Opt*, 6(2001)457; doi.org/10.1117/1.1411979
3. Nishidate I, Aizu Y, Mishina H, *J Biomed Opt*, 9(2004)700; doi.org/10.1117/1.1756918
4. Iwai T, Kimura G, *Opt Rev*, 7(2000)436-441;
5. Jacques S L, Saidu I S, Tittel F K, *Proc SPIE*, 2128(1994)231-237.
6. Nishidate I, Aizu Y, Mishina H, *Opt Rev*, 10(2003)427-435.
7. Masuda Y, Yamashita T, Hirao T, Takahashi M, *Skin Res Technol*, 15(2009)224-229; doi.org/10.1111/j.1600-0846.2009.00359.x
8. Wang L, Jacques S L, Zheng L Q, *Comput Methods Programs Biomed*, 47(1995)131-146.
9. Maeda T, Arakawa N, Takahashi M, Aizu Y, *Opt Rev*, 17(2010)223-229.
10. Van Gemert M J C, Jacques S L, Sterenborg H J C M, Star W M, *IEEE Trans Biomed Eng*, 36(1989)1146-1154.
11. Meglinski I V, Matcher S J, *Physiol Meas*, 23(2002)741; doi.org/10.1088/0967-3334/23/4/312
12. Meglinski I V, Matcher S J, *Comput Methods Programs Biomed*, 70(2003)179-186; doi.org/10.1016/S0169-2607(02)00099-8

[Received: 15.7.2018; accepted:1.11.2018]

**Prof Yoshihisa Aizu** received Dr. Eng. in electronics from Hokkaido University in 1985. From 1985 to 1989, he was in Kowa Company Limited, Tokyo. In 1989, he joined Hokkaido University as a research associate. From 1990, he was an associate professor at Muroran Institute of Technology, and in 2006 he was promoted a professor, the position he now holds. From 1992 to 1993, he was a visiting researcher in University Erlangen, Germany. His current research activities are in the fields of biomedical applications of spectroscopy, optical imaging, colorimetry, laser speckle imaging, and laser light scattering. He is a member of SPIE and OSA, and some Japanese Societies in the related fields.



**Kaustav DAS** completed B-Tech in biomedical engineering from Netaji Subhash Engineering College, Kolkata, India in 2015, and M-Tech in biomedical instrumentation from University of Calcutta, Kolkata, India in 2017. From 2018, he is a graduate student in Doctor Course and works as a research assistant in Optical Instrumentation Laboratory, Muroran Institute of Technology, Japan. His research areas are biomedical optics and biomedical instrumentation.



**Hideki Funamizu** is an associate professor in the Division of Production Systems Engineering, Muroran Institute of Technology. He received his BE, ME and Ph D degrees in electronics and information engineering from Hokkai-Gakuen University in 2003, 2005, and 2008, Japan. From 2008 to 2010, he was an assistant professor in Tokyo University of Science. In 2010, he joined Muroran Institute of Technology. His current research activities are in the fields of the biomedical optical imaging, digital holographic technique and speckle measurements. He is a member of OSA, SPIE, and three Japanese Societies in the related fields.



**Yuta KOBORI** received the B. Eng., in mechanical engineering from Muroran Institute of Technology in 2017. He is now a graduate student in Master Course, Muroran Institute of Technology. His research area is optical measurement techniques of biological objects including numerical simulations of light propagation in human skin.



**Dr Takaaki Maeda** received the B. Eng., Ms. Eng., and Dr. Eng. in mechanical engineering from Muroran Institute of Technology, in 2004, 2006, and 2009, respectively. From 2009 to 2010, he was a post-doctoral researcher in the Optical Instrumentation Laboratory, Muroran Institute of Technology. In 2010, he joined the Mechanical Engineering Department, Kushiro National College of Technology, Hokkaido Japan, as a research associate, and now he is an associate professor there. His current research activities are in the fields of biomedical optical imaging, colorimetry, and spectroscopic measurements. He is a member of some Japanese Societies in the related fields.



**Prof Tomonori Yuasa** joined Muroran Institute of Technology as a research associate in 1992. In 2004, he received Dr. Eng. in mechanical engineering from Muroran Institute of Technology. From 2006, he was an associate professor at Muroran Institute of Technology. From 1996 to 1997, he was a visiting researcher in Royal Institute of Technology, Sweden, and VTT Information Technology, Finland. His current research activities are in the fields of image processing, colorimetry, database and networking. He is a member of some Japanese Societies in the related fields.

